Intermolecular Hydrogen Bonding in Chlorine Dioxide Photochemistry: A Time-Resolved Resonance Raman Study

ARTICLE *in* CHEMICAL PHYSICS · JANUARY 2001

Impact Factor: 1.65 · DOI: 10.1016/S0301-0104(00)00370-0

4 AUTHORS, INCLUDING:

Matthew Philpott
University of Washington Seattle
8 PUBLICATIONS **200** CITATIONS
SEE PROFILE

Carsten L. Thomsen
NKT Photonics A/S
59 PUBLICATIONS **778** CITATIONS
SEE PROFILE

ELSEVIER

Chemical Physics 263 (2001) 389–400

Chemical Physics

www.elsevier.nl/locate/chemphys

Intermolecular hydrogen bonding in chlorine dioxide photochemistry: A time-resolved resonance Raman study

Matthew P. Philpott, Sophia C. Hayes, Carsten L. Thomsen [1], Philip J. Reid *

Department of Chemistry, University of Washington, Box 351700, Seattle, WA 98195-1700, USA

Received 8 August 2000

Abstract

The geminate-recombination and vibrational-relaxation dynamics of chlorine dioxide (OClO) dissolved in ethanol and 2,2,2-trifluoroethanol (TFE) are investigated using time-resolved resonance Raman spectroscopy. Stokes spectra are measured as a function of time following photoexcitation using degenerate pump and probe wavelengths of 398 nm. For OClO dissolved in ethanol, subpicosecond geminate recombination occurs resulting in the reformation of ground-state OClO with a quantum yield of 0.5 ± 0.1. Following recombination, intermolecular-vibrational relaxation of OClO occurs with a time constant of 31 ± 10 ps. For OClO dissolved in TFE, recombination occurs with a time constant of 1.8 ± 0.8 ps and a quantum yield of only 0.3 ± 0.1. The intermolecular-vibrational-relaxation time constant of OClO in TFE is 79 ± 27 ps. The reduced geminate-recombination quantum yield, delayed recombination, and slower vibrational relaxation for OClO in TFE is interpreted in terms of greater self-association of the solvent. Degenerate pump–probe experiments are also presented that demonstrate decay of the Cl-solvent charge-transfer complex on the ~1-ns time scale in ethanol and TFE. This time is significantly longer than the abstraction times observed for other systems demonstrating that Cl hydrogen abstraction from alcohols occurs in the presence of a significant energy barrier.

1. Introduction

Determining how solvents influence geminate-recombination and vibrational-relaxation dynamics is central to understanding chemical reactivity in condensed media [1–3]. Attempts to achieve this understanding have focused on the dynamics of diatomic solutes, with the majority of studies in this area focusing on I_2 [4–16]. These studies have shown that the photoinitiated dissociation of I_2 is followed by subpicosecond geminate recombination of the nascent photofragments resulting in the reformation of I_2. [2] The excess vibrational energy contained by I_2 is lost to the solvent through intermolecular-vibrational relaxation [5]. The efficiency of geminate recombination is dependent on the initial collisional dynamics between the photofragments and surrounding solvent molecules (i.e., the solvent cage); however, subpicosecond recombination has been observed for a variety of systems consistent with the rate of

* Corresponding author.

E-mail address: preid@chem.washington.edu (P.J. Reid).

[1] Present address: Department of Chemistry, University of Åarhus, Langelandsgade 140 DK-8000 Åarhus C, Denmark.

[2] The term "geminate recombination" is taken to mean recombination of the photofragments from the same precursor consistent with the nomenclature presented in Ref. [5].

0301-0104/01/$ - see front matter
PII: S0301-0104(00)00370-0

recombination being relatively insensitive to the details of the solvent [5,17]. I_2 intermolecular-vibrational relaxation proceeds on the tens-to-hundreds of picoseconds time scale depending on environment [4,5]. The rate of relaxation has been well modeled using isolated-binary-collision theory consistent with short-range forces dominating the solvent–solute interaction dynamics.

A more complex picture of geminate recombination and vibrational relaxation has emerged for charged and/or polar diatomics where electrostatic as well as collisional solvent–solute interactions become important. This complexity is well illustrated by recent studies of I_2^- [18–22]. Here, the geminate-recombination quantum yield in water is two and four times greater than in ethanol or acetonitrile, respectively [19]. The specific solvent–solute interactions responsible for variation of the geminate-recombination quantum yield are not well understood at present. The vibrational-relaxation time constant for I_2^- in water is 2.8 ps, but increases to 4.5 ps in ethanol and acetonitrile [18,19,22–25]. Comparison of these times to the relaxation times of I_2 outlined above demonstrates that the relaxation of I_2^- is substantially accelerated. Through comparison with MD simulations, this acceleration has been assigned to the presence of electrostatic solvent–solute interactions that are enhanced by "charge-flow" accompanying vibrational motion [20,21]. Studies of other diatomic systems such as ClO^- [26], CN^- [26,27] and polar HgI [28,29] have also found vibrational-relaxation times that are shorter than expected if only collisional dynamics were operative, further supporting the importance of electrostatic coupling for charged or polar species in solution [30].

Recently, there has been a great deal of interest in extending the description of geminate recombination and vibrational relaxation developed from studies of diatomic systems to triatomics. Barbara and coworkers have observed slow geminate recombination (3.5 ps) and extremely fast vibrational relaxation ($\ll$3.5 ps) for aqueous O_3^-, and have attributed these effects to strong electrostatic interactions [31]. Studies by Hochstrasser and coworkers have found that the vibrational-relaxation time constant for N_3^- dissolved in water, deuterated water, methanol, or ethanol is $<$3 ps [32]. In contrast, the vibrational-relaxation time constant in polar, aprotic hexamethyl-phosphamide is $\sim$15 ps consistent with intermolecular hydrogen bonding accelerating the rate of vibrational relaxation [32]. Studies of I_3^- dissolved in cooled and glassy ethanol have shown that the quantum yield for recombination increases with a reduction in temperature consistent with increased rigidity of the solvent shell [33]. Finally, recent studies by Keiding and coworkers on aqueous CS_2 have demonstrated that vibrational relaxation occurs on the tens-of-picoseconds time scale, substantially slower than the times observed for charged triatomics in solution [34]. In addition, the efficient (93%) geminate recombination of the CS and S photofragments has been assigned to solvent-assisted internal conversion [34]. In summary, these studies indicate that for small molecular systems in solution, the efficiency of geminate recombination and the rate of intermolecular vibrational relaxation are strongly dependent on the specific solvent–solute interactions that are operative.

Chlorine dioxide (OClO) represents an excellent opportunity to extend our understanding of triatomic reactivity in condensed environments. This compound has been of recent interest due to its involvement in a variety of stratospheric photochemical processes [35]. OClO is a 19-electron neutral radical that is isoelectronic with O_3^-. Photoexcitation into the $^2B_1$–$^2A_2$ electronic transition ($\lambda_{max} \sim 360$ nm) results in population of the predissociative $^2A_2$ state. Internal conversion from this state to the $^2A_1$ state is followed by subsequent internal conversion to the $^2B_2$ state from which photoproduct production is believed to occur [35]. The partitioning between photoproduct channels is environment dependent, and recent femtosecond pump–probe and time-resolved resonance Raman (TRRR) studies have been performed to elucidate the solvent–solute dynamics responsible for this dependence [36–45]. These experiments have demonstrated that subpicosecond geminate recombination of the primary photoproducts occurs resulting in the reformation of vibrationally excited ground-state OClO. In addition, Cl formation occurs through a bifurcated process with the 'prompt' production of Cl accompanied by delayed production on the $\sim$200-ps time scale via

decomposition of ground-state ClOO [36,37]. Solvent-dependence studies have shown that both the geminate-recombination quantum yield and intermolecular-vibrational relaxation rate are substantially reduced in acetonitrile relative to water, and this observation has lead to the hypothesis that intermolecular hydrogen-bonding represents a substantial component of solvent–solute coupling [41,43].

Progress in defining the solvent–solute interactions that influence the geminate-recombination and vibrational-relaxation dynamics of OClO, and triatomics in general, is dependent on performing studies in which specific aspects of the solvent response are isolated and systematically modified. Towards this end, we present a series of subpicosecond TRRR studies of OClO dissolved in ethanol and 2,2,2-trifluoroethanol (TFE). When combined with our previous studies of aqueous OClO, the results presented here provide the opportunity to investigate the influence of intermolecular hydrogen bonding on the reaction dynamics of OClO. Stokes spectra are obtained as a function of time following photolysis using degenerate pump and probe wavelengths of 398 nm. In ethanol, subpicosecond geminate recombination resulting in the production of ground-state OClO occurs with a quantum yield of 0.5 ± 0.1. Following recombination, the intermolecular-vibrational relaxation of OClO proceeds with a time constant of $\sim$30 ps. In contrast, the time constant for geminate recombination in TFE is $\sim$1.8 ps, significantly delayed relative to any other solvent studied to date. In addition, the geminate-recombination quantum yield is only 0.3 ± 0.1. The vibrational-relaxation time constant for OClO dissolved in TFE is $\sim$80 ps, significantly longer compared to water or ethanol. The reduced geminate-recombination quantum yield, delayed recombination, and slower vibrational relaxation in TFE is interpreted in terms of the propensity of this solvent to exist as a monomer (referred to as "self-association" in this paper) as well as stabilization of the photofragments through solvent complexation. Degenerate pump–probe studies are also presented in which substantial long-time ($\sim$1 ns) changes in optical density are observed in ethanol and TFE consistent with decay of the Cl-solvent charge-transfer complex via hydrogen abstraction. This rate of abstraction rate is substantially smaller than the rates observed for other systems suggesting that hydrogen abstraction from alcohols occurs in the presence of a significant energy barrier.

2. Materials and methods

The laser spectrometer has been described in detail elsewhere [41]. Briefly, a home-built Ti:sapphire oscillator pumped by an argon-ion laser (operating all-lines) produced 30-fs pulses (full-width at half-maximum) centered at 795 nm at a repetition rate of 91 MHz. The pulses were amplified by a Ti:sapphire regenerative amplifier (Clark-MXR CPA-1000-PS) providing 700 μJ pulses tunable from 770 to 810 nm at a repetition rate of 1 kHz. The 398-nm pump and probe beams were generated by frequency doubling the 795-nm amplifier output in a 1-mm thick β-BBO crystal (Type I). The polarization of the pump was rotated to 54.7° relative to the probe using a zero-order half-wave plate to minimize the contribution of rotational dynamics to the data. The photoinitiated evolution in optical density at 398 nm was measured using standard pump–probe techniques described elsewhere [41]. In the pump–probe studies, 10-mM solutions of OClO dissolved in the solvent of interest were delivered to a 2-mm path length, fused-silica flow cell. The synthesis of OClO has been described elsewhere [46]. Pulse energies of 4 and $>$0.5 μJ were employed for the pump and probe, respectively. Pump and probe beam waists at the sample were 1 mm and 350 μm, respectively. All intensities were determined to scale linearly with pump and probe intensity. Flow rates of $\sim$100 ml min^{-1} were employed ensuring that each pump–probe sequence interrogated a fresh sample volume. The instrument response as measured by the optical Kerr effect in water and was 750 ± 50 fs.

For the TRRR studies, pulse energies of 4 and 0.9 μJ were employed for the pump and probe, respectively. A 135° backscattering geometry was employed, with the beams focused onto a 2-mm path-length fused-silica flow cell containing 30-mM OClO solutions. Spatial overlap of the pump

and probe was optimized by monitoring the pump-induced depletion of ground-state OClO using a photodiode located behind the sample. The scattered light was collected with standard, refractive UV-quality optics and delivered to a 0.5-m focal-length spectrograph (Acton 505F) equipped with a 2400 grooves mm^{-1} holographically ruled grating. Spectrometer slit widths were adjusted to provide ~ 15 cm^{-1} resolution. The scattered light was detected by a liquid nitrogen-cooled, 1340×100 pixel, back-thinned, CCD detector (Princeton Instruments). The instrument response as measured by the optical Kerr effect in water was 1.2 ± 0.1 ps. The time resolution employed here is reduced relative to previous studies; however, this reduction was necessary in order to reduce spectral overlap between OClO and solvent transitions. The time-resolved difference spectra presented here were constructed as follows. At each time delay, three Raman spectra were obtained with the "probe only", "pump and probe", and the "pump only" incident on the sample. Six-minute integration times were employed for each spectrum. The pump-only spectrum was subtracted from the pump-and-probe to produce the "probe-with-photolysis" spectrum. The probe-only spectrum then was subtracted from the probe-with-photolysis spectrum to produce the difference spectra reported here.

The time-dependent evolution in optical density or scattered intensity was analyzed by fitting the data to a convolution of the instrument response with a sum of exponentials using the Levenberg–Marquardt algorithm. A minimal number of exponentials were employed to produce an accurate fit, with goodness of fit determined by the reduced χ^2 values and visual inspection of the residuals. Error values represent one standard deviation from the mean. The error bars on the TRRR data represent one standard deviation from the mean.

3. Results

3.1. Static absorption spectra

Fig. 1 presents the absorption spectra of OClO dissolved in water, ethanol, and TFE. The absorption in this wavelength region corresponds to the $^2B_1$–$^2A_2$ transition [35]. Absorption band maxima are located at 358 ± 1 nm in water, 360 ± 1 nm in ethanol, and 357 ± 1 nm in TFE, with all values in agreement with previous work [47]. The absorption band maximum has been shown to correlate with the free energy of solvation for a variety of solvents [47]. However, TFE deviates significantly from this correlation suggesting that specific intermolecular interactions such as hydrogen bonding are operative in this solvent [47]. The broadening evident in the absorption spectrum is clearly solvent dependent; however, the subtle variation of the absorption-band maxima suggests that the relative energy of the $^2B_1$ and $^2A_2$ states is only weakly solvent dependent. Similar conclusions have been reached for OClO dissolved in cyclohexane, water, and chloroform [46,48].

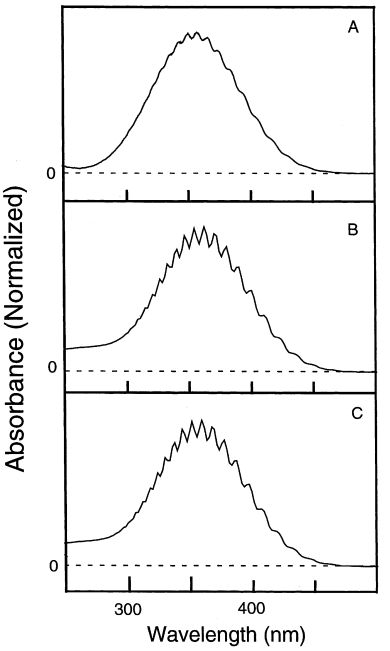

Fig. 1. Absorption spectra of OClO dissolved in (A) water, (B) ethanol, and (C) TFE.

3.2. 398-nm degenerate pump–probe

Pump–probe studies were performed since the interpretation of the TRRR data is simplified

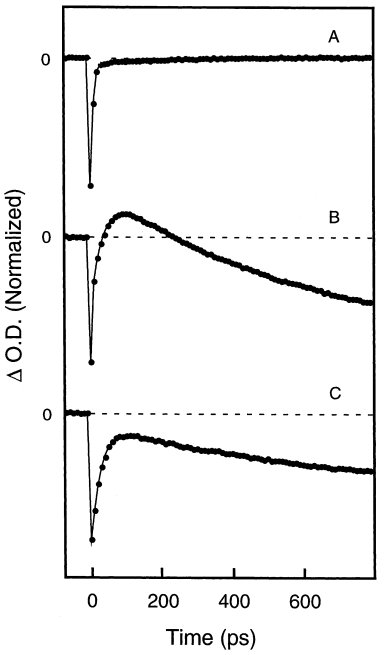

Fig. 2. Pump–probe dynamics at long-time delays for OClO dissolved in (A) water, (B) ethanol, and (C) TFE. Pump and probe wavelengths are 398 nm. The solid line corresponds to the best fit to the data as described in the text, with parameters corresponding to this fit presented in Table 1.

when the magnitude and time scale of optical-density evolution in the wavelength region of interest is known. Fig. 2 presents the time-dependent change in optical density measured at 398 nm following OClO photoexcitation. Two species are expected to contribute to the optical-density evolution at this wavelength: OClO formed by geminate recombination, and the Cl-solvent charge-transfer complex [49]. On the time scale investigated here, an instrument-response-limited reduction in optical density is observed in all solvents consistent with the depletion of ground-state OClO through photoexcitation. The subsequent recovery of the optical-density depletion is extremely solvent dependent. [3] In water, this recovery was best fit using two time constants of 6.9 ± 1.3 and 340 ± 180 ps, with the kinetic parameters determined from this analysis presented in Table 1. The early-time recovery in optical density has been shown to originate from the reformation and subsequent vibrational relaxation of ground-state OClO [38,39,41,42], where the later-time optical density evolution arises from Cl-solvent charge-transfer complex formation [36,37]. A long-time offset in optical density was also included in the kinetic analysis. The amplitude of this component was 0.03 ± 0.02 in water, with the observation of positive optical density at long times demonstrating that the Cl-water charge-transfer complex is stable on the time scale investigated here.

In contrast to the dynamics observed in water, the long-time evolution in optical density observed in ethanol and TFE is consistent with decomposition of the Cl-solvent charge-transfer complex on the ~1-ns time scale. In ethanol and TFE (Fig. 2B and C), the initial depletion in optical density recovers with a time-constant of 22.5 ± 1.5 and 25.8 ± 1.5 ps, respectively. This initial recovery is followed by a decay in optical density occurring with time constants of 890 ± 100 ps in ethanol and 1120 ± 680 ps in TFE. The decay in optical density is consistent with decomposition of the Cl-solvent charge-transfer complex, presumably through hydrogen abstraction. This process is expected to result in the formation of HCl consistent with the observation that the ethanol and TFE samples became appreciably more acidic over time. In addition, the amplitude of the kinetic component assigned to the charge-transfer complex is larger in ethanol and TFE relative to water (Table 1) demonstrating that at this probe wavelength, the absorption cross-section of the charge-transfer complex is substantially larger in the alcohols. The Cl-solvent charge-transfer absorption band maximum is dependent on the ionization potential of the solvent [50], with the ionization potentials of ethanol (10.64 eV) [51] and TFE (11.49 eV) [52] being lower than that of water (12.62 eV) [51]. The lower ionization potential for ethanol and TFE combined with the ~310-nm absorption-band maximum of the Cl-water charge-transfer complex [49] suggests that the absorption cross-section of

[3] It should be noted that the early-time recovery in optical density observed in aqueous solution is more complicated than the analysis presented here indicates. See Refs. [30,40,42,46] for a more detailed discussion of these dynamics.

Table 1
Kinetic parameters for 398-nm degenerate pump–probe

	A_1[a]	τ_1 (ps)	A_2	τ_2 (ps)	A_3	τ_3 (ps)
Water	-0.91 ± 0.03	6.9 ± 1.3	-0.06 ± 0.02	340 ± 180	0.03 ± 0.02	Offset[b]
Ethanol	-0.29 ± 0.03	22.5 ± 1.5	0.40 ± 0.02	890 ± 100	-0.31 ± 0.02	Offset
TFE	-0.37 ± 0.04	25.8 ± 1.5	0.30 ± 0.03	1120 ± 680	-0.33 ± 0.03	Offset

[a] Amplitudes are normalized such that $\sum |A_i| = 1$. Errors represent one standard deviation from the mean.
[b] A time constant of 10 000 ps was included to represent any persistent offset in optical density at long delay times.

the Cl-solvent charge-transfer complex should be substantial at 398 nm in both ethanol and TFE thereby supporting the assignment of the long-time evolution in optical density to decay of the Cl-solvent complex.

3.3. Time-resolved resonance Raman: Chloride dioxide in ethanol

Fig. 3 presents TRRR Stokes difference spectra of OClO in ethanol. In the 0-ps difference spectrum, a reduction in the intensity of the OClO symmetric-stretch fundamental and overtone transitions is observed consistent with ground-state depletion created by photolysis. Apparent derivative intensity is observed for the 886 cm^{-1} line of ethanol. This intensity is absent when the pump and probe are not overlapped in time, and the presence of a pump field can result in vibrational lineshape modulation [53]. However, similar effects are not observed in "solvent-only" experiments. Furthermore, the positive intensity occurs at $\sim$850 cm^{-1} consistent with ClO formation at early times, with the decay of this intensity within the instrument response being consistent with rapid geminate recombination (see below). As the delay between the pump and probe increases, the extent of OClO depletion decreases up to $\sim$80 ps consistent with the reformation of ground-state OClO through geminate recombination. Comparison of the initial depletion amplitude to the depletion that persists at later delays establishes that the geminate-recombination quantum yield in ethanol is 0.5 ± 0.1. It should be noted that the substantial evolution in optical density corresponding to the Cl-solvent charge-transfer complex combined with uncertainty in the absorption cross-section of this complex prohibits determination of the geminate-recombination quantum yield from the pump–probe data. The geminate-recombination quantum yield in ethanol is substantially reduced relative to water (0.90 ± 0.10) [43]. To avoid interpretive difficulties arising from overlap of the OClO symmetric-stretch fundamental transition and the 886 cm^{-1} solvent, kinetic

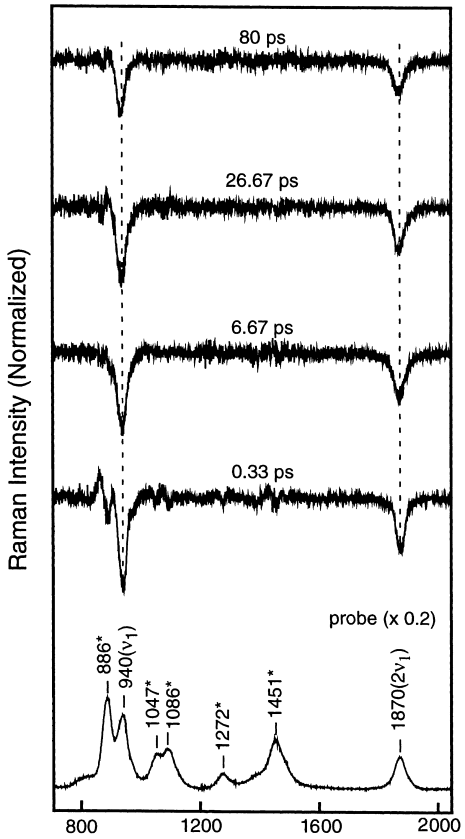

Fig. 3. TRRR Stokes difference spectra of OClO dissolved in ethanol. Pump and probe wavelengths are 398 nm. The time delay between the pump and probe for a given spectrum is indicated. The probe-only spectrum is presented at the bottom of the figure. Ethanol transitions are marked with an asterisk in the probe-only spectrum.

analysis was performed using the intensity of the symmetric-stretch overtone transition at 1870 cm^{-1} (Fig. 4A). Inspection of the temporal evolution in depletion intensity (Fig. 4A) demonstrates that the recovery in scattered intensity is biphasic. Consistent with this observation, the data were best modeled by a sum of three exponentials convolved with the instrument response resulting in recovery time constants of 0.3 ± 0.1 ps (instrument-response limited), 31 ± 10 ps, and a fixed offset representing the long-time depletion. The instrument response limited reformation of ground-state OClO is similar to behavior observed in water and acetonitrile [43]. In addition, the later time recovery has been shown to correspond to the vibrational relaxation of OClO [43]. Compared to the 9-ps relaxation time observed in water, the ~30-ps time observed in ethanol demonstrates that

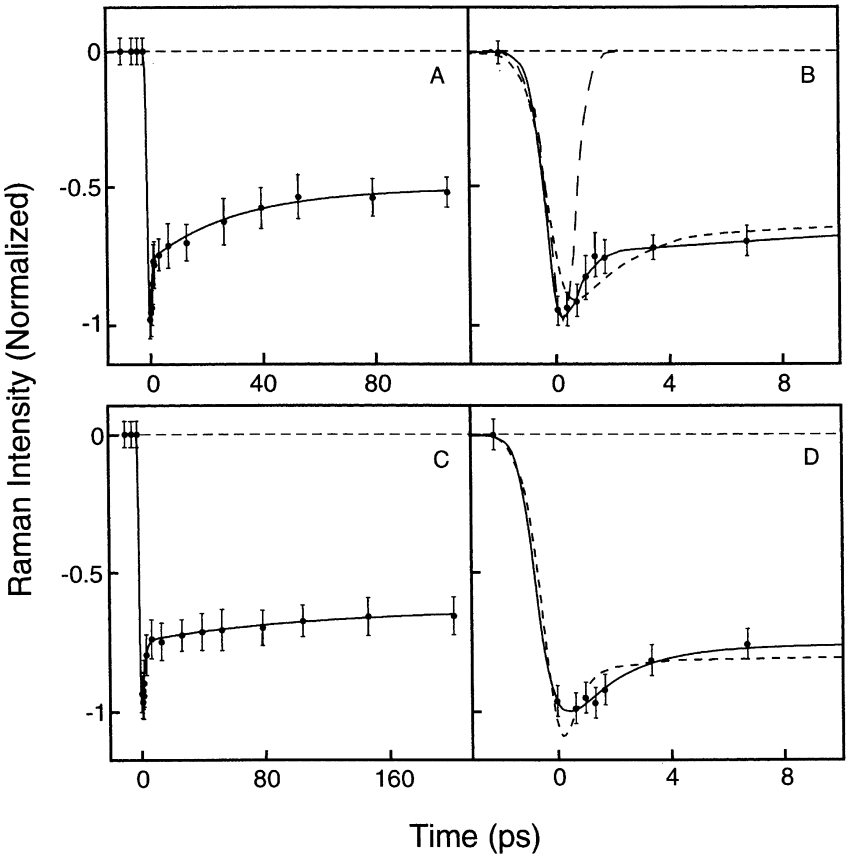

Fig. 4. (A) Intensity of the OClO symmetric-stretch overtone Stokes transition as a function of time for OClO in ethanol at 398 nm. Best fit to the data by the sum of three exponentials convolved with the instrument response is given by a solid line corresponding to times of 0.3 ± 0.1 ps (normalized amplitude of -0.82 ± 0.05), 31 ± 10 ps (-0.06 ± 0.03), and a long-time offset (-0.12 ± 0.04). (B) Expanded view of the early time recovery in Stokes intensity presented in panel A. The best fit to the data as described above is presented as the solid line. The dashed line represents the best fit when the shortest time constant is held to 1.8 ps as described in the text. The instrument response is given by the long-dashed line centered at 0-ps delay. (C) Intensity of the OClO symmetric-stretch overtone Stokes transition in 2,2,2-trifluoroethanol as a function of time. Best fit to the data by the sum of three exponentials convolved with the instrument response is given by a solid line corresponding to times of 1.8 ± 0.8 ps (normalized amplitude of -0.39 ± 0.08), 31 ± 10 ps (-0.07 ± 0.04), and long-time offset (-0.54 ± 0.08). (D) Expanded view of the early time recovery in Stokes intensity presented in panel C. The best fit to the data as described above is presented as the solid line. The dashed line represents the best fit when the shortest time constant is held to 0.3 ps as described in the text.

the intermolecular-vibrational-relaxation rate is substantially reduced in this solvent.

3.4. Time-resolved resonance Raman: OClO in 2,2,2-trifluoroethanol

Fig. 5 presents TRRR Stokes difference spectra of OClO dissolved in TFE. At 0-ps delay, negative intensity is observed for OClO transitions consistent with photoinduced ground-state depletion. In addition, negative intensity observed for the 830-cm^{-1} transition of TFE implying that the optical density of the sample has increased; however, the sample optical density is actually decreased as demonstrated by the pump–probe data (Fig. 2). Furthermore, the intensity of this transition is not derivative, as was the case in ethanol. Finally, negative solvent intensity persists for delays outside the pump–probe temporal overlap. All of these observations are inconsistent with pump-pulse induced frequency modulation of the solvent transition, and we will argue below that this intensity arises from strong interaction between OClO and the solvent. Compared to the 0-ps spectrum, the depletion in OClO scattered intensity decreases for delays up to 150 ps consistent with reformation of ground-state OClO through geminate recombination. Fig. 4C displays the integrated intensity of the OClO symmetric-stretch overtone transition as a function of delay. The residual depletion observed at longer delays relative to the initial depletion is consistent with a geminate-recombination quantum yield of 0.3 ± 0.1 in TFE. Best fit to the temporal evolution in OClO scattered intensity was accomplished using two recovery time constants of 1.8 ± 0.8, 79 ± 27 ps, and a fixed offset representing the long-time scattering depletion. The ~80-ps recovery time demonstrates that the intermolecular-vibrational-relaxation rate for OClO dissolved in TFE is significantly reduced relative to water or ethanol. In addition, the 1.8-ps recovery time is substantially longer than the instrument-response limited recovery observed in all other solvents studied to date demonstrating that the rate of geminate recombination is reduced in this solvent. However, the limited number of data points obtained in this time region requires critical evaluation of this result. Fig. 4B presents a comparison of the best fit to the ethanol data described above to a fit where the early-time recovery is fixed to be 1.8 ps. For this later fit, χ^2 is ~8 times larger than that of the best fit. Fig. 4D presents a comparison between the best fit to the TFE data and a fit where the early-time constant is fixed to 0.3 ps. Compared to the best fit, χ^2 increases by an order of magnitude. The comparative analyses presented in Fig. 4B and D suggest that the rate of geminate recombination is indeed reduced in TFE. Dramatic support for this result is found in Fig. 5

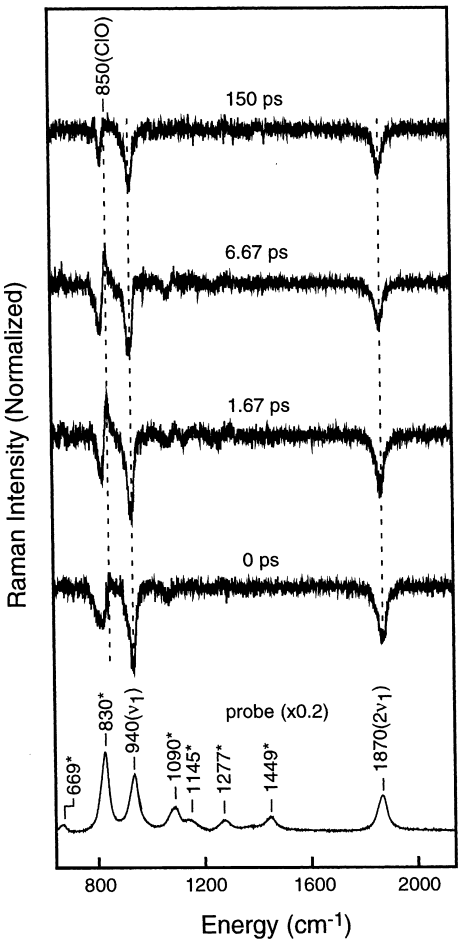

Fig. 5. Time-resolved Stokes resonance Raman difference spectra of OClO in TFE. The delay between the pump and probe for a given spectrum is indicated. The probe-only spectrum is presented at the bottom of the figure. The transitions of TFE are marked with an asterisk in the probe-only spectrum.

where positive intensity is observed at 850 cm^{-1} consistent with ClO formation. Analysis of the ClO scattering intensity is not possible due to overlap with the solvent scattering; however, the presence of positive intensity in this frequency region suggests that ClO is indeed produced as a stable photoproduct following OClO photoexcitation

4. Discussion

4.1. Geminate recombination

The TRRR data presented here provide limited support for a correlation between geminate-recombination efficiency and intermolecular hydrogen bonding. The geminate-recombination quantum yields in ethanol (~0.5) and TFE (~0.3) are substantially reduced compared to water (~0.9) consistent with the modulation of intermolecular hydrogen bonding in these solvents. Quantitative comparison of intermolecular-hydrogen-bonding strengths can be performed using the Kalmut–Taft α-scale [54]. The α parameter is one of a collection of solvochromatic parameters that correlates specifically with the hydrogen-bond donating strength of the solvent. According to this scale, water ($\alpha = 1.17$) is a better hydrogen-bond donating solvent than ethanol ($\alpha = 0.86$) consistent with the larger geminate-recombination quantum yield in water. However, the high α-value of TFE ($\alpha = 1.51$) does not translate into efficient geminate recombination. The correlation between hydrogen-bonding strength and geminate recombination is compromised in TFE by the propensity for this solvent to exist as a monomer compared to the polymeric structures favored by water and ethanol [55,56]. This tendency towards self-association arises from the ability of TFE to form an intramolecular hydrogen bond between the hydroxyl proton and the electrophilic CF_3 group [57]. This self-association is also reflected by the modest hydrogen-bond-accepting ability of this solvent, a behavior that would further frustrate intermolecular bonding [54]. Therefore, the geminate-recombination quantum yields observed here suggest that it is not simply the ability of the solvent to form an intermolecular hydrogen bond with the solute, but the propensity of the solvent to form polymeric structures through intermolecular hydrogen bonding that is important for efficient geminate recombination. The existence of solvent-intermolecular structure could enhance recombination in two ways. First, the translational energy required to break through the solvent cage would be increased in the presence of substantial intermolecular hydrogen bonding. Second, the presence of intermolecular bonding could increase the photofragments/solvent collisional cross-section over that of an isolated monomer. Enhanced geminate recombination with greater solvent intermolecular bonding is consistent with recent studies of I_3^- in ethanol [33]. In this work, a reduction in temperature from 300 to 150 K resulted in a substantial increase in the geminate-recombination quantum yield. In ethanol, polymer formation is enhanced with a reduction in temperature such that the correlation between solvent-cage rigidity and intersolvent bonding is reasonable [58].

It should be noted that the TRRR studies in TFE suggest that the dynamics in this solvent may be unique such that comparison with other solvents must be performed with caution. The delayed recombination in TFE combined with the observation of ClO scattering in this solvent suggests that following photodissociation, the primary photofragments are stabilized through solvent/photofragment complexation. In addition, the depletion and recovery in TFE scattering intensity at 830 cm^{-1} indicates that it may be more appropriate to envision photoexcitation of a OClO–TFE complex rather than weakly solvated OClO. There is some precedence for solvent–solute complexation occurring in halogenated solvents. For example, delayed geminate recombination has been observed for excited-state I_2 [12]. Here, a delay in the formation of A'-state I_2 following photoexcitation was observed, with the length of this delay increasing with the strength of the I/solvent complex. Complexation of ClO has been observed in studies of OClO dissolved in benzene where formation of the ClO/benzene charge-transfer complex was observed [59]. Therefore, complexation of ClO and/or O with TFE may be largely responsible for the reduced recombination in this solvent.

The observation of ClO scattering in TFE combined with the absence of corresponding intensity in any other solvent studied to date supports existing models of OClO photochemistry in which photoexcitation leads to the formation of a distorted OClO that undergoes ground-state internal conversion [38,39]. In this model, evolution along the reaction coordinate approaching the ClO/O asymptote results in the formation of distorted OClO on the $^2B_2$ surface. Collision with the solvent results in efficient internal conversion to the ground state before complete dissociation. A similar picture has recently emerged to explain the geminate-recombination dynamics of I_2 in condensed environments [16]. The absence of ClO intensity in water combined with the observation of intensity in TFE suggests that the extent of ClO formation following the photoexcitation of aqueous OClO is modest. However, the absence of ClO scattering in ethanol and acetonitrile [43], solvents where the extent of cage escape is also appreciable, severely compromises this conclusion. The absorption maximum of ClO in aqueous solution is ~280 nm such that resonant enhancement of this species in these experiments is not expected [49]. Given this, it is the observation of ClO scattering in TFE that should be viewed as surprising. It is possible that the absorption spectrum of ClO in TFE is shifted to lower frequency resulting in resonant enhancement. In addition, thermal excitation of ClO is also expected to affect the scattering cross-section such that the differences in ClO intensity may be due to solvent-dependent vibrational relaxation dynamics. Finally, the ClO intensity in TFE may be due to resonance enhancement arising from the ClO/solvent charge-transfer complex. Differentiation between these models can be made through femtosecond pump–probe studies as well as TRRR studies utilizing probe wavelengths that are resonant with ClO. Such experiments are currently underway.

4.2. Hydrogen abstraction

The results presented here demonstrate that in ethanol and TFE, decay of the Cl-solvent charge-transfer complex occurs on the ~1-ns time scale, substantially longer than the times observed in other halogen-solvent abstraction reactions. Time-resolved infrared absorption studies by Hochstrasser and coworkers have shown that hydrogen-abstraction from alkanes by Cl occurs on the ~10-ps time scale [60]. In addition, studies of hydrogen abstraction from chloroform by CN, also performed by Hochstrasser and coworkers, found that efficiency of abstraction is significantly reduced in solution relative to the gas phase. The tens-of-picoseconds time scale observed for this abstraction was ascribed to a reduction in abstraction rate accompanying the slower rotational reorganization of chloroform in solution. However, the absence of knowledge concerning the structural reorganization dynamics of the Cl/solvent complexes of interest here prohibits any prediction of the abstraction rate. It should be noted though that ~1-ns^{-1} rate observed here is significantly longer than the rates observed for other systems suggesting that Cl hydrogen abstraction from alcohols occurs in the presence of a substantial barrier. An estimate for this barrier can be made assuming thermalization of the Cl-solvent complex, and that the abstraction process is well modeled as unimolecular. In this limit, the ~1-ns^{-1} rate observed here translates into a energy barrier to abstraction of 2.7 kcal mol^{-1} (Arrhenius pre-exponential factor of 10^{11} s^{-1}).

4.3. Chlorine dioxide vibrational relaxation

The results presented here, combined with those of previous studies, demonstrate that the rate constant for OClO vibrational relaxation is solvent dependent. Previous TRRR anti-Stokes studies found that OClO intermolecular-vibrational relaxation occurs in ~9 ps in water and ~33 ps in acetonitrile [43]. The increased vibrational relaxation rate in water relative to acetonitrile was proposed to arise from solvent–solute hydrogen bonding. Here, the vibrational-relaxation time in ethanol is ~30 ps, similar to the time scale observed in acetonitrile. The similarity in relaxation time constants between ethanol and acetonitrile apparently invalidates simple correlation between enhanced vibrational relaxation and intermolecular hydrogen bonding. However, the symmetric stretch (918 cm^{-1}) and methyl-rock (1124 cm^{-1}) modes of acetonitrile are well matched to the

OClO symmetric (945 cm^{-1}) and asymmetric stretch (1100 cm^{-1}) modes such that the coupling between OClO and acetonitrile is expected to be appreciable, and the ~30-ps relaxation time in acetonitrile may be an upper limit for polar, aprotic solvents. In TFE, the ~80-ps vibrational relaxation time constant is the longest relaxation time for solution-phase OClO observed to date. We propose that the protracted vibrational relaxation time in TFE is due to the inefficiency of intermolecular hydrogen bonding in this solvent. As mentioned above, TFE undergoes a high degree of self-association such that the extent in intermolecular hydrogen bonding is less than expected from the Kalmut–Taft α-value. In addition, the OClO symmetric-stretch (ν_1) frequency is sensitive to intermolecular hydrogen bonding. For example, the symmetric-stretch fundamental transition is observed at 945 cm^{-1} in water, but decreases to 938 cm^{-1} in acetonitrile and cyclohexane [43,46,48]. The frequency of this transition is 940 cm^{-1} in both ethanol and TFE, consistent with modest intermolecular hydrogen bonding in both solvents. It should be noted that the variation in the vibrational relaxation time determined from TRRR could be due to solvent dependence of the scattering cross-sections; however, the similarities of the electronic absorption spectra (Fig. 1) suggest that this is probably not the case.

Acknowledgements

The National Science Foundation is acknowledged for their support of this work through the CAREER program (CHE-9701717). Support from the Petroleum Research Fund administered by the American Chemical Society is acknowledged. P.J.R. is a Cottrell Fellow of the Research Corporation and an Alfred P. Sloan Fellow. C.L.T. gratefully acknowledges the support of the University of Åarhus for financial support.

References

[1] D.W. Oxtoby, Adv. Chem. Phys. 47 (1981) 487.
[2] J.C. Owrutsky, D. Raftery, R.M. Hochstrasser, Ann. Rev. Phys. Chem. 45 (1994) 519.
[3] A. Laubereau, W. Kaiser, Rev. Mod. Phys. 50 (1978) 607.
[4] M.E. Paige, C.B. Harris, Chem. Phys. 149 (1990) 37.
[5] A.L. Harris, J.K. Brown, C.B. Harris, Ann. Rev. Phys. Chem. 39 (1988) 341.
[6] T.J. Chuang, G.W. Hoffman, K.B. Eisenthal, Chem. Phys. Lett. 25 (1974) 201.
[7] P. Bado, C. Dupuy, D. Magde, K.R. Wilson, M.M. Malley, J. Chem. Phys. 80 (1984) 5531.
[8] R. Zadoyan, Z. Li, P. Ashjian, C.C. Martens, V.A. Apkarian, Chem. Phys. Lett. 218 (1994) 504.
[9] Y.-J. Yan, R.M. Whitnell, K.R. Wilson, A.H. Zewail, Chem. Phys. Lett. 193 (1992) 402.
[10] D.J. Nesbitt, J.T. Hynes, J. Chem. Phys. 77 (1982) 2130.
[11] X. Xu, S.-C. Yu, R. Lingle, H. Zhu, J.B. Hopkins, J. Chem. Phys. 95 (1991) 2445.
[12] R.J. Lingle, X. Xu, S.-C. Yu, H. Zhu, J.B. Hopkins, J. Chem. Phys. 93 (1990) 5667.
[13] N.F. Scherer, L.D. Ziegler, G.R. Fleming, J. Chem. Phys. 96 (1992) 5544.
[14] N.F. Scherer, D.M. Jonas, G.R. Fleming, J. Chem. Phys. 99 (1993) 153.
[15] B. Otto, J. Schroeder, J. Troe, J. Chem. Phys. 81 (1984) 202.
[16] V.S. Batista, D.F. Coker, J. Chem. Phys. 105 (1996) 4033.
[17] B.J. Schwartz, J.C. King, J.Z. Zhang, C.B. Harris, Chem. Phys. Lett. 203 (1993) 503.
[18] D.A.V. Kliner, J.C. Alfano, P.F. Barbara, J. Chem. Phys. 98 (1993) 5375.
[19] P.K. Walhout, J.C. Alfano, K.A.M. Thakur, P.F. Barbara, J. Phys. Chem. 99 (1995) 7568.
[20] I. Benjamin, R. M Whitnell, Chem. Phys. Lett. 204 (1993) 45.
[21] I. Benjamin, P.F. Barbara, B.J. Gertner, J.T. Hynes, J. Phys. Chem. 99 (1995) 7557.
[22] T. Kühne, P. Vöhringer, J. Chem. Phys. 105 (1996) 10788.
[23] U. Banin, A. Waldman, S. Ruhman, J. Chem. Phys. 96 (1992) 2416.
[24] U. Banin, S. Ruhman, J. Chem. Phys. 98 (1993) 4391.
[25] S. Hess, H. Bürsing, P. Vöhringer, J. Chem. Phys. 111 (1999) 5461.
[26] P. Hamm, M. Lim, R.M. Hochstrasser, J. Chem. Phys. 107 (1997) 10523.
[27] E.J. Heilweil, F.E. Doany, R. Moore, R.M. Hochstrasser, J. Chem. Phys. 76 (1982) 5632.
[28] N. Pugliano, A.Z. Szarka, S. Gnanakaran, M. Triechel, R.M. Hochstrasser, J. Chem. Phys. 103 (1995) 6498.
[29] S. Gnanakaran, R.M. Hochstrasser, J. Chem. Phys. 105 (1996) 3486.
[30] R.M. Whitnell, K.R. Wilson, J.T. Hynes, J. Chem. Phys. 96 (1992) 5354.
[31] P.K. Walhout, C. Silva, P.F. Barbara, J. Phys. Chem. 100 (1996) 5188.
[32] M. Li, J. Owrutsky, M. Sarisky, J.P. Culver, A. Yodh, R.M. Hochstrasser, J. Chem. Phys. 98 (1993) 5499.
[33] Z. Wang, T. Wasserman, E. Gershgoren, J. Vala, R. Kosloff, S. Ruhman, Chem. Phys. 313 (1999) 155.

[34] C.L. Thomsen, D. Madsen, J. Thogersen, J.R. Byberg, S.R. Keiding, J. Chem. Phys. 111 (1999) 703.
[35] V. Vaida, J.D. Simon, Science 268 (1995) 1443.
[36] C.L. Thomsen, P.J. Reid, S.R. Keiding, J. Am. Chem. Soc. in press.
[37] J. Thogersen, C.L. Thomsen, J.Aa. Poulsen, S.R. Keiding, J. Phys. Chem. A 102 (1998) 4186.
[38] C.L. Thomsen, S.R. Keiding, J. Thogersen, J.Aa. Poulsen, J. Chem. Phys. 108 (1998) 8461.
[39] J. Thorgersen, P.U. Jepsen, C.L. Thomsen, J.R. Byberg, S.R. Keiding, J.Aa. Poulsen, J. Phys. Chem. 101 (1997) 3317.
[40] C.L. Thomsen, M.P. Philpott, S.C. Hayes, P.J. Reid, J. Chem. Phys. 112 (2000) 505.
[41] M.J. Philpott, S. Charalambous, P.J. Reid, Chem. Phys. 236 (1998) 207.
[42] M.J. Philpott, S. Charalambous, P.J. Reid, Chem. Phys. Lett. 281 (1997) 1.
[43] S.C. Hayes, M.P. Philpott, S.G. Mayer, P.J. Reid, J. Phys. Chem. A 103 (1999) 5534.
[44] S.C. Hayes, M.J. Philpott, P.J. Reid, J. Chem. Phys. 109 (1998) 2596.
[45] Y.J. Chang, J.D. Simon, J. Phys. Chem. 100 (1996) 6406.
[46] A. Esposito, C. Foster, R. Beckman, P.J. Reid, J. Phys. Chem. A 101 (1997) 5309.
[47] R.C. Dunn, B.N. Flanders, V. Vaida, J.D. Simon, Spectrochim. Acta 48A (1992) 1293.
[48] C.E. Foster, P.J. Reid, J. Phys. Chem. A 102 (1998) 3541.
[49] U.K. Kläning, T. Wolff, Ber. Bunsenges. Phys. Chem. 89 (1985) 243.
[50] J.E. Chateauneuf, Chem. Phys. Lett. 164 (1989) 577.
[51] K. Kimura, S. Iwata, T. Yamazaki, Y. Achiba, S. Katsumata, Handbook of Photoelectron Spectra of Fundamental Organic Molecules, Halsted Press, New York, 1981.
[52] I. Koppel, U. Molder, R. Pikver, Org. React. Tartu 20 (1983) 45.
[53] B. Dick, R.M. Hochstrasser, Chem. Phys. 75 (1983) 133.
[54] M.J. Kamlet, J.-L.M. Abboud, M.H. Abraham, R.W. Taft, J. Org. Chem. 48 (1983) 2877.
[55] A. Kivinen, J. Murto, Suomen Kemistilehti 40 (1967) 6.
[56] R. Laenen, C. Rauscher, J. Chem. Phys. 107 (1997) 9759.
[57] T. Radnai, S. Ishigoro, H. Ohtaki, J. Solut. Chem. 18 (1989) 771.
[58] F. Schwager, E. Marand, R.M. Davis, J. Phys. Chem. 100 (1996) 19268.
[59] Y.I. Dakhnovskii, R. Doolen, J.D. Simon, J. Chem. Phys. 101 (1994) 6640.
[60] D. Raftery, M. Iannone, C.M. Phillips, R.M. Hochstrasser, Chem. Phys. Lett. 201 (1993) 513.